

Accurate and stable time stepping in ice sheet modeling

Gong Cheng¹, Per Lötstedt¹ and Lina von Sydow¹

¹Division of Scientific Computing, Department of Information Technology, Uppsala University, Uppsala, Sweden

Abstract

In this paper we introduce adaptive time step control for simulation of evolution of ice sheets. The discretization error in the approximations is estimated using “Milne’s device” by comparing the result from two different methods in a predictor-corrector pair. Using a predictor-corrector pair the expensive part of the procedure, the solution of the velocity and pressure equations, is performed only once per time step and an estimate of the local error is easily obtained. The stability of the numerical solution is maintained and the accuracy is controlled by keeping the local error below a given threshold using PI-control. Depending on the threshold, the time step Δt is bound by stability requirements or accuracy requirements. Our method takes a shorter Δt than an implicit method but with less work in each time step and the solver is simpler. The method is analyzed theoretically with respect to stability and applied to the simulation of a 2D ice slab and a 3D circular ice sheet. The stability bounds in the experiments are explained by and agree well with the theoretical results.

1 Introduction

There is a growing interest in the prediction of the evolution of the large ice sheets on Antarctica and Greenland and their contribution to the future sea level rise [1, 2, 3, 4]. Simulations of the dynamics of ice sheets in the past and in the future have been made, see e.g. [5, 6], but improvements in the modeling and the numerical methods are required for better fidelity, accuracy, and efficiency [7]. In this paper, we introduce a method to automatically choose the time steps to control the discretization error and stability of the time integration of the governing system of partial differential equations (PDEs).

The full Stokes (FS) equations for the velocity field in the ice and an advection equation for the evolution of the ice surface are regarded as an accurate

model of the motion of glaciers and ice sheets [8, 9, 10]. The viscosity in the FS equations depends non-linearly on the velocity. The numerical solution of the equations is therefore demanding in terms of computational time. Hence, different simplifications of the FS equations have been derived under various assumptions to reduce the computing effort. The shallow ice approximation (SIA) is based on the assumption that the thickness of the ice in the vertical direction is small compared to a length scale in the horizontal direction [8]. Other approximations are the shallow shelf approximation (SSA) [11, 10] and the Blatter-Pattyn model [12, 13]. Comparisons between solutions of the FS equations and the SIA equations are found in [14, 15, 16]. The Ice Sheet Coupled Approximation Levels (ISCAL) is an adaptive method using SIA or FS in different parts of the ice sheet [17, 18].

Numerical models have been implemented in codes for simulation of large ice sheets. They are often using a finite element method for the FS equations or approximations of them as in [19, 20, 21, 22, 23] or a finite volume method as in [24]. The PDE to evolve the thickness of the ice is time dependent and in the discretization of the time derivative a time step Δt has to be chosen for accuracy and stability. The stability of a class of one-step schemes with a θ -parameter for the time derivative has been analyzed in [25]. Restrictions on Δt are derived by Fourier analysis of the linearized equations. If Δx is the distance between the nodes in the space discretization then $\Delta t \leq C_* \Delta x^2$ for some constant C_* . These one-step schemes are applied to large ice sheets in [26].

The discretization of the PDE in space gives a system of ordinary differential equations (ODEs). In the numerical solution of initial value problems for ODEs, the time step is often chosen to control the estimated local error in the time discretization [27, 28, 29]. Given the error estimate and the present time step, a new time step is selected to the next time point such that an error tolerance is satisfied and the solution remains stable [30].

We introduce adaptive time step control for simulation of the ice sheet equations in the community ice sheet model Elmer/Ice [19]. Then the time step varies in the time interval of interest and there is no need to guess a stable and sufficiently accurate Δt for the whole interval in the beginning of the simulation. Spatial derivatives are approximated by the finite element method in Elmer/Ice. The mesh is extruded in the vertical direction from a triangular or quadrilateral mesh in the horizontal plane. It is adjusted in every time step to follow the free boundary at the ice surface. The dominant part of the computational effort is spent on the solution of the equations for the velocity and the pressure in the ice.

The discretization error in the approximations is estimated using “Milne’s device” by comparing the result from two different methods in a predictor-corrector pair of Adams type of first and second order accuracy in time

[31, 27]. The advantage with a predictor-corrector pair is that the expensive part of the procedure, the solution of the velocity and pressure equations, is performed only once per time step and that an estimate of the local error is easily obtained. The time step Δt is chosen to fulfill an error tolerance using PI control according to Söderlind [30]. There is a bound on Δt depending on Δx^2 as in [25]. An unconditionally stable method would allow longer Δt but also require a fully implicit method and the solution of several different velocity equations in the iterations to compute the solution in every time step.

The outline of the paper is as follows. The equations that govern the evolution of the ice sheets are stated in Section 2. The predictor method is the Forward Euler method or the second order Adams-Bashforth method and the corrector method is the Backward Euler method or the second order Adams-Moulton method (also referred to as the trapezoidal method) [27] or simplifications of them. The methods are combined in Section 3 to solve for the velocities using FS, SIA, or ISCAL and the advection equation for the thickness. In Section 4, the time step control is introduced. The stability of the methods applied to the thickness equation with the velocity from the SIA equation is analyzed as in [25] in Section 5. In Section 6, the stability of the predictor-corrector scheme is investigated. The time step control is tested in Section 7 by simulation over long time intervals of examples in two and three dimensions from [17, 32, 33] using the SIA, FS, and ISCAL solvers in Elmer/Ice [17, 19]. Conclusions are drawn in the final Section 8.

2 Equations governing the ice sheet dynamics

In this section we describe the equations and solvers for the flow of ice sheets.

2.1 The full Stokes (FS) equations

The flow of an ice sheet can be modeled by the non-linear FS equations [9]. These equations are defined by balance of mass

$$\nabla \cdot \mathbf{v} = 0, \tag{1}$$

balance of momentum

$$\rho \dot{\mathbf{v}} = -\nabla p + \nabla \cdot \mathbf{T}^D + \rho \mathbf{g}, \tag{2}$$

and a constitutive equation, the so called Glen's flow law

$$\mathbf{D} = \mathcal{A}(T') f(\sigma) \mathbf{T}^D. \tag{3}$$

Here \mathbf{v} is the vector of velocities $\mathbf{v} = (v_x \ v_y \ v_z)^{\mathbf{T}}$, ρ is the density of the ice and p is the pressure. The deviatoric stress tensor \mathbf{T}^D is given by

$$\mathbf{T}^D = \begin{pmatrix} t_{xx}^D & t_{xy}^D & t_{xz}^D \\ t_{yx}^D & t_{yy}^D & t_{yz}^D \\ t_{zx}^D & t_{zy}^D & t_{zz}^D \end{pmatrix}, \quad (4)$$

where t_{xx}^D , t_{yy}^D , t_{zz}^D and t_{xy}^D denote longitudinal stresses and t_{xz}^D , t_{yz}^D vertical shear stresses. We also have symmetry $t_{xy} = t_{yx}$, $t_{xz} = t_{zx}$ and $t_{yz} = t_{zy}$. The gravitational acceleration in the z -direction is denoted by \mathbf{g} , and the total time derivative of the velocity by $\dot{\mathbf{v}}$ which is very small and neglected in glaciological applications. Glen's flow law (3) relates the stress and strain rate, where $\mathbf{D} = \frac{1}{2}(\nabla\mathbf{v} + (\nabla\mathbf{v})^{\mathbf{T}})$ is the strain rate tensor and $\mathcal{A}(T')$ the rate factor that describes how the viscosity depends on the pressure melting point corrected temperature T' . For isothermal flow, the rate factor \mathcal{A} is constant. Finally,

$$f(\sigma) = \sigma^2 \quad (5)$$

is the creep response function for ice where σ is the effective stress defined by

$$\sigma^2 = (t_{xx}^D)^2 + (t_{yy}^D)^2 + (t_{zz}^D)^2 + \frac{1}{2}((t_{xx}^D)^2 + (t_{yy}^D)^2 + (t_{zz}^D)^2). \quad (6)$$

With the viscosity η defined by

$$\eta = (2\mathcal{A}f(\sigma))^{-1}, \quad (7)$$

the FS equations (1), (2) and (3) describing the flow of a non-Newtonian fluid can be written

$$\begin{aligned} \nabla \cdot (\eta(\nabla\mathbf{v} + \nabla\mathbf{v}^{\mathbf{T}})) - \nabla p + \rho\mathbf{g} &= 0, \\ \nabla \cdot \mathbf{v} &= 0. \end{aligned} \quad (8)$$

If the ice base is frozen, the velocity \mathbf{v} satisfies a no slip condition at the base

$$\mathbf{v} = 0. \quad (9)$$

An ice sliding at the base is modeled by a sliding law [34]. Let \mathbf{I} be the identity matrix. At the surface with normal \mathbf{n} , the ice is stress free with

$$(-p\mathbf{I} + \mathbf{T}^D) \cdot \mathbf{n} = 0. \quad (10)$$

The FS equations (1) and (8) are discretized in space by a finite element method with linear P1-P1 elements with stabilization to avoid spurious oscillations in the pressure using the standard setting in Elmer/Ice [19]. The resulting system of non-linear equations is solved by Newton iterations. The system of linear equations in every Newton iteration is solved iteratively.

2.2 The Shallow Ice Approximation (SIA)

The SIA is derived from FS by scaling of variables and perturbation expansions, see e.g. [8, 35]. The underlying assumption is that the aspect ratio ε of the ice sheet – the quotient between the thickness H and a length scale L of the ice sheet – is small. The SIA velocities and pressure can be computed from the following expressions (using v_{xb} and v_{yb} as the basal sliding velocities, the Euclidean vector norm $\|\cdot\|_2$, and $g = \|\mathbf{g}\|_2$)

$$\begin{aligned}
 v_x &= v_{xb} - 2(\rho g)^3 \frac{\partial h}{\partial x} \|\nabla h\|_2^2 \int_b^z \mathcal{A}(h-s)^3 ds, \\
 v_y &= v_{yb} - 2(\rho g)^3 \frac{\partial h}{\partial y} \|\nabla h\|_2^2 \int_b^z \mathcal{A}(h-s)^3 ds, \\
 v_z &= - \int_b^z \left(\frac{\partial v_x}{\partial x} + \frac{\partial v_y}{\partial y} \right) ds, \\
 p &= \rho g(h-z).
 \end{aligned} \tag{11}$$

In [14, 36] the validity and accuracy of SIA were examined. Due to the assumptions in the derivation of SIA it does not perform well in regions with large spatial variations in data, at steep margins, in ice streams, in ice shelves, and at domes.

2.3 The Ice Sheet Coupled Approximation Levels (ISCAL)

While FS is an accurate model for ice sheet flow, it is computationally expensive to solve. SIA on the other hand is computationally cheap, but fails to compute accurate solutions in large regions of the ice sheet for realistic glaciological applications. For this reason, FS and SIA were coupled into ISCAL and implemented in Elmer/Ice in [17]. This method decides automatically and dynamically where SIA is valid and use this approximation in these regions. FS is employed for the remaining part of the ice sheet where a more accurate solver is required. This way the overall computational complexity is substantially reduced compared to FS, still being much more accurate than SIA. ISCAL was applied to a simplified ice sheet covering Svalbard in [18].

2.4 The free surface equation and the thickness equation

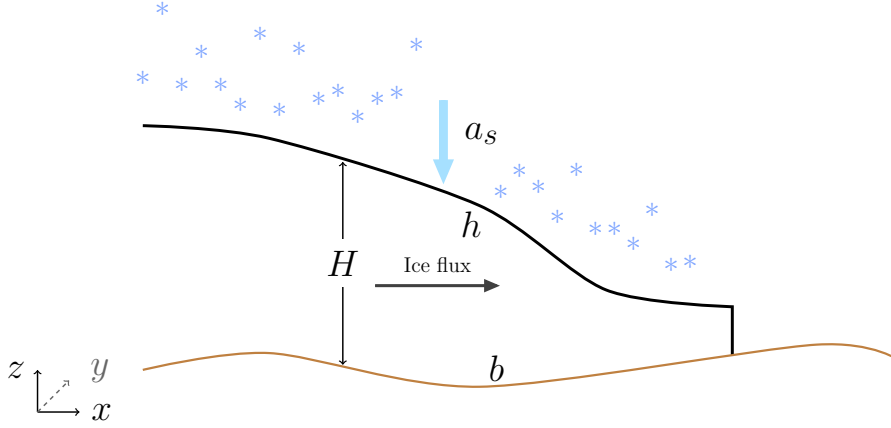


Figure 1: An ice sheet with height h , bedrock elevation b , thickness H , and accumulation a_s .

The z -coordinate of the free surface position $h(x, y, t)$ (see Figure 1) is given by the free surface equation

$$\frac{\partial h}{\partial t} + v_x \frac{\partial h}{\partial x} + v_y \frac{\partial h}{\partial y} - v_z = a_s, \quad (12)$$

where a_s denotes the net surface accumulation/ablation. As an alternative to solving this equation for $h(x, y, t)$, we can solve the thickness advection equation

$$\frac{\partial H}{\partial t} + \frac{\partial q_x}{\partial x} + \frac{\partial q_y}{\partial y} = a_s \quad (13)$$

for $H(x, y, t) = h(x, y, t) - b(x, y)$ (see Figure 1). The z -coordinate of the ice base is $b(x, y)$. In (13), the flux is

$$q_x = \int_b^h v_x dz, \quad q_y = \int_b^h v_y dz. \quad (14)$$

Both the free surface (12) and the thickness (13) equation are solved in one dimension lower than the velocity equation. In this paper, we will use the thickness equation (13) to compute the time evolution of the ice sheet. A stabilization term is added to the equation making the spatial discretization behave like an upwind scheme according to the direction of the velocity.

3 Time stepping

We will use a predictor-corrector time stepping scheme for (13), rewritten as

$$\frac{\partial H}{\partial t} = a_s - \frac{\partial q_x}{\partial x} - \frac{\partial q_y}{\partial y} = f(H, v). \quad (15)$$

The numerical approximation of H at time t_n , $n \geq 0$, is H^n and the time step is $\Delta t_n = t_n - t_{n-1}$.

The predictor-corrector algorithm becomes

1. **Predictor step:** Solve for \tilde{H}^n explicitly in time from v^{n-1} , H^{n-1} , H^{n-2} , etc.
2. **Velocity solver:** Solve for v^n using the predictor \tilde{H}^n .
3. **Corrector step:**
 - Fully implicit scheme: Solve for H^n implicitly from v^n , H^n , H^{n-1} , H^{n-2} , etc.
 - Semi-implicit scheme: Solve for H^n implicitly from v^n , \tilde{H}^n , H^{n-1} , H^{n-2} , etc.

The velocities in Step 2 can be computed using either FS, SIA, or ISCAL.

We consider both a first order predictor step using Forward Euler (FE)

$$\tilde{H}^n = H^{n-1} + \Delta t_n f(H^{n-1}, v^{n-1}), \quad (16)$$

and the second order Adams-Bashforth method (AB)

$$\tilde{H}^n = H^{n-1} + \Delta t_n [\beta_1^n f(H^{n-1}, v^{n-1}) + \beta_2^n f(H^{n-2}, v^{n-2})], \quad (17)$$

where

$$\zeta^n = \frac{\Delta t_n}{\Delta t_{n-1}}, \quad \beta_1^n = 1 + \frac{\zeta^n}{2}, \quad \beta_2^n = -\frac{\zeta^n}{2}.$$

For the corrector step, the fully implicit and semi-implicit Backward Euler are considered as first order accurate methods

$$H^n = H^{n-1} + \Delta t_n f(H^n, v^n), \quad (18)$$

$$H^n = H^{n-1} + \Delta t_n f(\tilde{H}^n, v^n), \quad (19)$$

denoted (FBE) and (SBE), respectively. The fully implicit Adams-Moulton (FAM)

$$H^n = H^{n-1} + \frac{\Delta t_n}{2} [f(H^n, v^n) + f(H^{n-1}, v^{n-1})], \quad (20)$$

and semi-implicit Adams-Moulton (SAM)

$$H^n = H^{n-1} + \frac{\Delta t_n}{2} \left[f(\tilde{H}^n, v^n) + f(H^{n-1}, v^{n-1}) \right], \quad (21)$$

are the second order methods considered.

Four different predictor-corrector schemes are listed in Table 1.

Scheme	Predictor	Corrector
FE-FBE	FE, Equation (16)	FBE, Equation (18)
FE-SBE	FE, Equation (16)	SBE, Equation (19)
AB-FAM	AB, Equation (17)	FAM, Equation (20)
AB-SAM	AB, Equation (17)	SAM, Equation (21)

Table 1: The four predictor-corrector schemes considered.

The first time step at $t = 0$ is taken by the first order method. In all the other time steps, the solution is advanced by the first or the second order method.

The schemes FE-FBE and AB-FAM are only used in the analysis, see Section 6. In Section 7, numerical results using FE-SBE and AB-SAM are presented.

4 Time step control

In each time step, we will compute a new Δt_{n+1} with the following algorithm:

- **Error estimate:** Estimate the local truncation error τ^n .
- **Adaptive time step:** Compute Δt_{n+1} from Δt_n , the local truncation errors τ^n, τ^{n-1} , and a given tolerance ϵ using a PI controller from [30].

FE (16) has the local error between the analytical solution $H(t_n)$ with initial data H^{n-1} and the numerical solution

$$H(t_n) - \tilde{H}^n = c_P \Delta t_n^2 H''(t_n) + \mathcal{O}(\Delta t_n^3) \quad , \quad c_P = \frac{1}{2}, \quad (22)$$

while SBE (19) has the local error

$$H(t_n) - H^n = c_I \Delta t_n^2 H''(t_n) + \mathcal{O}(\Delta t_n^3) \quad , \quad c_I = -\frac{1}{2}. \quad (23)$$

Combining (22) and (23) gives the following leading term of the local truncation error for SBE

$$\tau^n = \frac{c_I(H^n - \tilde{H}^n)}{\Delta t_n(c_I - c_P)} = \frac{1}{2\Delta t_n}(H^n - \tilde{H}^n). \quad (24)$$

From (24) we compute the next time step using PI.4.2 in [30]

$$\Delta t_{n+1} = \left(\frac{\epsilon}{\eta_n}\right)^{\beta_1} \left(\frac{\epsilon}{\eta_{n-1}}\right)^{\beta_2} \Delta t_n, \quad n = 1, 2, \dots, \quad (25)$$

where $\eta = \max_{\Omega} |\tau^n|$ over the spatial domain Ω with parameters $\beta_1 = 3/10$ and $\beta_2 = -1/10$ suggested in [30].

Similarly, we have for the second order method that AB in (17) has local error

$$H(t_n) - \tilde{H}^n = c_P(\zeta^n) \Delta t_n^3 H''' + \mathcal{O}(\Delta t_n^4) \quad , \quad c_P(\zeta^n) = \frac{1}{6} + \frac{1}{4\zeta^n}, \quad (26)$$

and SAM in (21) has local error

$$H(t_n) - H^n = c_I \Delta t_n^3 H''' + \mathcal{O}(\Delta t_n^4) \quad , \quad c_I = -\frac{1}{12}. \quad (27)$$

Again, combining the expressions for the local errors gives the following local truncation error for SAM

$$\tau^n = \frac{c_I(H^n - \tilde{H}^n)}{\Delta t_n(c_I - c_P)} = \frac{\zeta^n(H^n - \tilde{H}^n)}{(3\zeta^n + 3)\Delta t_n}, \quad (28)$$

and the new time step using PI.4.2 is given by (25) with $\beta_1 = 1/5$ and $\beta_2 = -1/15$, see [30].

5 Analysis of a simplified 2D-problem

A stability analysis for a 2D-problem is performed using SIA in this section. The analysis follows [25], but our final results are slightly more comprehensive.

5.1 Analytical expressions

For a 2D-problem, we derive by (11) and the no-slip condition that the SIA-velocities are given by

$$\begin{aligned} v_x &= -\frac{1}{2} \mathcal{A}(\rho g)^3 \left(\frac{\partial h}{\partial x}\right)^3 (H^4 - (h-z)^4), \\ v_z &= \frac{1}{2} \mathcal{A}(\rho g)^3 \left\{ 4 \left(\frac{\partial h}{\partial x}\right)^3 \left[H^3 \frac{\partial H}{\partial x} (z-b) + \frac{1}{4} \frac{\partial h}{\partial x} ((h-z)^4 - H^4) \right] + \right. \\ &\quad \left. + 3 \left(\frac{\partial h}{\partial x}\right)^2 \left[H^4 (z-b) - \frac{1}{5} (H^5 - (h-z)^5) \right] \frac{\partial^2 h}{\partial x^2} \right\}. \end{aligned} \quad (29)$$

The average velocity in the vertical direction is denoted by \bar{v} . Use (14) and $C = \frac{2}{5}\mathcal{A}(\rho g)^3$ to obtain

$$\bar{v} = \frac{q_x}{H} = \frac{\int_b^h v_x dz}{H} = -CH^4 \left(\frac{\partial h}{\partial x} \right)^3. \quad (30)$$

Using this in (13) gives

$$\frac{\partial H}{\partial t} + \frac{\partial(\bar{v}H)}{\partial x} = a_s, \quad (31)$$

which can also be written as an equation related to a p -parabolic equation with $p = 4$ [37]

$$\frac{\partial H}{\partial t} - \frac{\partial}{\partial x} \left(CH^5 \left| \frac{\partial h}{\partial x} \right|^2 \frac{\partial h}{\partial x} \right) = a_s. \quad (32)$$

In general, an ice sheet model is a coupled system consisting of equations for velocities, thickness, temperature, grounding-line migration, and bedrock motion. Numerically, these equations are usually solved separately in a time step keeping the variables from the other equations constant. For instance, we use a fixed H at the current time step when we solve for the velocity \bar{v} and then use the fixed \bar{v} to solve for the evolution of the thickness H . In the analysis of the time discretization of the thickness equation (32), there are two different sources of H : one from the calculation of the velocity \bar{v} denoted by \hat{H} and one from the integration of the thickness equation written H . Then, the new thickness equation is

$$\frac{\partial H}{\partial t} - \frac{\partial}{\partial x} \left(C\hat{H}^4 \left| \frac{\partial \hat{h}}{\partial x} \right|^2 \frac{\partial \hat{h}}{\partial x} H \right) = a_s. \quad (33)$$

The coupled system (33) is linearized by introducing the perturbation $\delta(x, t)$ about the steady state solution for the thickness $\bar{H}(x)$ and the height $\bar{h}(x)$. Then H and \hat{H} are expressed as

$$\begin{aligned} H &= \bar{H} + \delta = \bar{h} - b + \delta, \\ \hat{H} &= \bar{H} + \hat{\delta} = \bar{h} - b + \hat{\delta}, \end{aligned} \quad (34)$$

and after ignoring quadratic terms and higher in δ we arrive at

$$\frac{\partial \delta}{\partial t} = C \frac{\partial}{\partial x} \left[4\bar{H}^4 \left(\frac{\partial \bar{h}}{\partial x} \right)^3 \hat{\delta} + 3\bar{H}^5 \left(\frac{\partial \bar{h}}{\partial x} \right)^2 \frac{\partial \hat{\delta}}{\partial x} + \bar{H}^4 \left(\frac{\partial \bar{h}}{\partial x} \right)^3 \delta \right], \quad (35)$$

where the first two terms on the right hand side derive from \bar{v} , cf. [25].

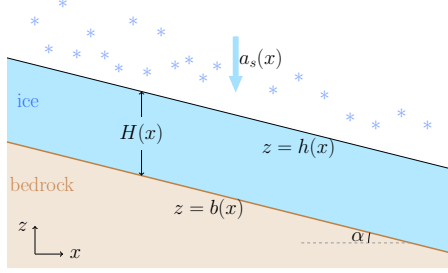


Figure 2: A slab-on-slope with time independent H and h .

In a slab-on-slope case (see Figure 2), we have a constant \bar{H} and $\frac{\partial b}{\partial x} = \frac{\partial \bar{h}}{\partial x} = \alpha$ and the model equation for δ is

$$\frac{\partial \delta}{\partial t} = 4C\alpha^3 \bar{H}^4 \frac{\partial \hat{\delta}}{\partial x} + 3C\alpha^2 \bar{H}^5 \frac{\partial}{\partial x} \left(\frac{\partial \hat{\delta}}{\partial x} \right) + C\alpha^3 \bar{H}^4 \frac{\partial \delta}{\partial x}, \quad (36)$$

Since the coefficient in front of the second derivative is positive, the solution δ is stable. In the next section, the thickness equation is discretized by an upwinding scheme and central differences are used for the derivative in the velocity solution. This is an equation modeling the time dependence of H in Elmer/Ice. The same result is obtained if (33) is first discretized and then linearized.

5.2 Stability analysis

The stability is investigated here when (36) is discretized in time using a θ -method with the time step Δt . When $\theta = 0$, the θ -method is the Forward Euler method and for $\theta > 0$, it is a mixed implicit/explicit method. In this analysis, $\hat{\delta}$ is always evaluated at the current time point.

First, we study Forward Euler in time with $\alpha < 0$ and centered and upwinding differences in space with step size Δx as described in Section 5.1. Let δ_j^n approximate $\delta(x_j, t_n)$ where $x_j = x_{j-1} + \Delta x$ and $t_n = t_{n-1} + \Delta t$. Then

$$\frac{\delta_j^{n+1} - \delta_j^n}{\Delta t} = 5C\alpha^3 \bar{H}^4 \frac{\delta_j^n - \delta_{j-1}^n}{\Delta x} + 3C\alpha^2 \bar{H}^5 \frac{\delta_{j+1}^n - \delta_{j-1}^n - \delta_j^n + \delta_{j-2}^n}{2\Delta x^2}. \quad (37)$$

Introducing

$$\xi = \frac{\Delta t}{\Delta x} \quad , \quad a = 5C\alpha^3 \bar{H}^4 \xi \quad , \quad c = \frac{3}{2}C\alpha^2 \bar{H}^5 \frac{\Delta t}{\Delta x^2}, \quad (38)$$

we arrive at

$$\delta_j^{n+1} = \delta_j^n + a (\delta_j^n - \delta_{j-1}^n) + c (\delta_{j+1}^n - \delta_j^n - \delta_{j-1}^n + \delta_{j-2}^n). \quad (39)$$

For the case $\alpha > 0$,

$$\delta_j^{n+1} = \delta_j^n + a (\delta_{j+1}^n - \delta_j^n) + c (\delta_{j+2}^n - \delta_{j+1}^n - \delta_j^n + \delta_{j-1}^n). \quad (40)$$

Replacing δ_k^n by the Fourier modes $\delta_\omega^n e^{ik\omega\Delta x}$ gives $\delta_\omega^{n+1} = \lambda \delta_\omega^n$ where λ is

$$\begin{aligned} \lambda &= 1 + |a|(\cos \omega\Delta x + i \sin \omega\Delta x - 1) + \\ &+ c(\cos 2\omega\Delta x + i \sin 2\omega\Delta x - 2i \sin \omega\Delta x - 1), \end{aligned} \quad (41)$$

considering both cases $\alpha < 0$ and $\alpha > 0$. For stability in the time discretization (39) and (40) for a given Δx , the requirement on λ is $|\lambda| \leq 1$ for all $\omega\Delta x \in [0, \pi]$. Let

$$k = \frac{|a|}{c} = \frac{10}{3} |\alpha| \frac{\Delta x}{\bar{H}}. \quad (42)$$

Then the restriction on the time step is (for details, see A)

$$\Delta t \leq \frac{k + 2 + 2\sqrt{k}}{2k^2 + 8} \frac{2\Delta x^2}{3C\alpha^2 \bar{H}^5}. \quad (43)$$

SIA is accurate when a typical length scale L in the horizontal direction is large compared to \bar{H} such that $\bar{H} = \varepsilon L$ with a small ε [14]. Then $k = 10|\alpha|\Delta x/(3\varepsilon L)$. When $\varepsilon \propto 0.01$, $\Delta x/L \propto 0.01 - 0.1$, and $\alpha \propto 0.01 - 0.1$, k will be $\propto 0.01 - 1$ and the factor with k in (43) is $\propto 1$, the bound on Δt will decrease with Δx^2 as expected with an explicit discretization of a parabolic equation (32) and decreases rapidly with increasing thickness as \bar{H}^{-5} . Only when k is large in (42), e.g. when the ice is very thin, we have $\Delta t \leq C_1 \Delta x / \bar{H}^4$ and longer time steps are possible. Compared to the bound in [25], the bound in (43) is sharp and more detailed.

A blend of the spatial first derivatives at two time levels is defined by a θ -parameter. Using the same notation as in (38) for a and c , the fully discretized scheme is for (36) with $\alpha < 0$

$$\begin{aligned} \delta_j^{n+1} - \delta_j^n &= c (\delta_{j+1}^n - \delta_{j-1}^n - \delta_j^n + \delta_{j-2}^n) \\ &+ a \left[(1 - \theta) (\delta_j^n - \delta_{j-1}^n) + \theta (\delta_j^{n+1} - \delta_{j-1}^{n+1}) \right]. \end{aligned} \quad (44)$$

The range of θ is $[0, \frac{1}{5}]$ since the first derivatives of δ are from two difference sources. As shown in (36), $\frac{\partial \delta}{\partial x}$ in the first and second terms of the right hand side are computed explicitly in the velocity equation and discretized in the previous time step. Therefore, only 1/5 of the first derivatives are determined by the θ -method. The remaining 4/5 of the first derivatives and the second derivative are always discretized explicitly in time. An implicit method, e.g. the Backward Euler method, applied only to the thickness equation is not a fully implicit method for the coupled system.

Again using Fourier analysis gives for the growth factor with $\theta \in [0, \frac{1}{5}]$

$$\lambda_\theta = \frac{[1 + c(\cos 2\omega\Delta x + i \sin 2\omega\Delta x - 2i \sin \omega\Delta x - 1) + |a|(1 - \theta)(\cos \omega\Delta x + i \sin \omega\Delta x - 1)]}{[1 - |a|\theta(\cos \omega\Delta x + i \sin \omega\Delta x - 1)]}. \quad (45)$$

Analytical bounds for Δt in (45) cannot be derived as easily as for Forward Euler in (43) when $\theta = 0$ in (44). Using the notation λ in (41), the growth factor for θ -method (45) is now

$$\lambda_\theta = \frac{\lambda - |a|\theta(\cos \omega\Delta x + i \sin \omega\Delta x - 1)}{1 - |a|\theta(\cos \omega\Delta x + i \sin \omega\Delta x - 1)}. \quad (46)$$

Let $z = |a|\theta(\cos \omega\Delta x + i \sin \omega\Delta x - 1)$ and \bar{z} is the complex conjugate of z . By simple calculation with the assumption above, we know that $|z| \ll 1$ and $\Re z \leq 0$. Then,

$$|\lambda_\theta| = \left| \frac{\lambda - z}{1 - z} \right| = \frac{|\lambda + |z|^2 - (z + \lambda\bar{z})|}{|1 - (z + \bar{z}) + |z|^2|} \leq |\lambda| + |z|^2 + |z|(1 + |\lambda|). \quad (47)$$

The bound on a stable Δt for the θ -method is in most cases more restricted than the bound for the explicit method. The exact bounds on Δt for stability for the θ -method can be computed numerically.

The separated procedure for velocity and thickness is a typical way of solving the coupled system. However, this is potentially problematic in ice sheet modeling since it tends to generate a diffusion term which is always solved explicitly in time. In Section 7.1, we compare numerical experiments with this analysis.

6 Stability analysis for the predictor-corrector schemes

The stability for (13) is analyzed here using the full predictor-corrector time stepping scheme in Section 3. The assumption is that $q_y = 0$ in (14) and that $q_x = \bar{v}H$ as in (30). The finite element discretization of the space derivative in (13) with linear hat functions in 1D is stabilized by adding a term proportional to the first derivative squared. On an equidistant mesh, the approximation corresponds to a finite difference discretization with upwinding for $\partial(\bar{v}H)/\partial x$.

Consider the predictor-corrector scheme AB-FAM, i.e. \tilde{H}^n is computed from (17), $\bar{v}^n = \bar{v}^n(\tilde{H}^n)$, and H^n is computed by (20) (see Table 1). Assuming that $\bar{v} > 0$, a_s is constant in time, and that \bar{H}^n is the steady state solution yields $\frac{\partial q_x^n}{\partial x} = \frac{\partial(\bar{v}^n \bar{H}^n)}{\partial x} = a_s$ and consequently

$$\bar{v}_j^k \bar{H}_j^k - \bar{v}_{j-1}^k \bar{H}_{j-1}^k = \Delta x a_s, \quad k = n, n-1. \quad (48)$$

Then by FAM $\bar{H}_j^{n+1} = \bar{H}_j^n$ and by AB $\tilde{H}_j^{n+1} = \bar{H}_j^n = \bar{H}_j^{n-1} = \tilde{H}_j^n$. Introduce as in Section 5.2 perturbations δ_j^n to the steady state at x_j denoted by \bar{H}_j in order to analyze the stability for these perturbations. FAM for $\bar{H}_j + \delta_j^{n+1}$ gives with ξ defined in (38)

$$\begin{aligned} & (\bar{H}_j + \delta_j^{n+1}) - (\bar{H}_j + \delta_j^n) + \\ & \frac{1}{2}\xi \left(\bar{v}_j(\bar{H} + \tilde{\delta}^{n+1})(\bar{H}_j + \delta_j^{n+1}) - \bar{v}_{j-1}(\bar{H} + \tilde{\delta}^{n+1})(\bar{H}_{j-1} + \delta_{j-1}^{n+1}) \right) + \\ & \frac{1}{2}\xi \left(\bar{v}_j(\bar{H} + \tilde{\delta}^n)(\bar{H}_j + \delta_j^n) - \bar{v}_{j-1}(\bar{H} + \tilde{\delta}^n)(\bar{H}_{j-1} + \delta_{j-1}^n) \right) = a_s. \end{aligned} \quad (49)$$

Linearize (49) ignoring quadratic terms in δ . We will also assume as in SIA that $\bar{v}_j(H)$ depends only locally on H_j as in (11), see B. Then use assumption (48) to arrive at

$$\begin{aligned} & \delta_j^{n+1} - \delta_j^n + \\ & \frac{1}{2}\xi \left(\bar{v}(\bar{H}_j)\delta_j^{n+1} - \bar{v}(\bar{H}_{j-1})\delta_{j-1}^{n+1} + \frac{\partial \bar{v}}{\partial H_j}(\bar{H}_j)\bar{H}_j\tilde{\delta}_j^{n+1} - \frac{\partial \bar{v}}{\partial H_{j-1}}(\bar{H}_{j-1})\bar{H}_{j-1}\tilde{\delta}_{j-1}^{n+1} \right) + \\ & \frac{1}{2}\xi \left(\bar{v}(\bar{H}_j)\delta_j^n - \bar{v}(\bar{H}_{j-1})\delta_{j-1}^n + \frac{\partial \bar{v}}{\partial H_j}(\bar{H}_j)\bar{H}_j\tilde{\delta}_j^n - \frac{\partial \bar{v}}{\partial H_{j-1}}(\bar{H}_{j-1})\bar{H}_{j-1}\tilde{\delta}_{j-1}^n \right) = 0. \end{aligned} \quad (50)$$

Assume that \bar{v} and $\frac{\partial \bar{v}}{\partial H_j}$ vary smoothly in space and time such that $\bar{v}(\bar{H}_j) - \bar{v}(\bar{H}_{j-1})$ and $\frac{\partial \bar{v}}{\partial H_j}(\bar{H}_j) - \frac{\partial \bar{v}}{\partial H_{j-1}}(\bar{H}_{j-1})$ are small. Introducing

$$\begin{aligned} \mu &= \frac{\partial \bar{v}}{\partial H_j}(\bar{H}_j)(1 - e^{-i\omega\Delta x}), \\ \nu &= \bar{v}(\bar{H}_j)(1 - e^{-i\omega\Delta x}), \end{aligned} \quad (51)$$

where $\omega\Delta x \in [0, \pi]$, and replacing δ_j^n and $\tilde{\delta}_j^n$ by the Fourier modes $\delta_\omega^n e^{ij\omega\Delta x}$ and $\tilde{\delta}_\omega^n e^{ij\omega\Delta x}$ in (50) gives

$$\delta_\omega^{n+1} - \delta_\omega^n + \frac{1}{2}\xi(\nu\delta_\omega^{n+1} + \mu\tilde{\delta}_\omega^{n+1} + \nu\delta_\omega^n + \mu\tilde{\delta}_\omega^n) = 0, \quad (52)$$

where both μ and ν are constant in time. For SIA it is known that $\frac{\partial \bar{v}}{\partial H_j} \propto \frac{1}{\Delta x}$ and $\mu \propto \frac{1}{\Delta x}$, see B, and there is reason to believe that $\frac{\partial \bar{v}}{\partial H_j}$ behaves similarly for the FS equation. Let $\gamma = 1/(1 + \frac{1}{2}\xi\nu)$ in (52) to obtain

$$\delta_\omega^{n+1} + \frac{1}{2}\xi\mu\gamma\tilde{\delta}_\omega^{n+1} = \gamma(1 - \frac{1}{2}\xi\nu)\delta_\omega^n - \frac{1}{2}\xi\gamma\mu\tilde{\delta}_\omega^n. \quad (53)$$

AB (17) for $\tilde{H}_j + \tilde{\delta}_j^{n+1}$ is defined by

$$\begin{aligned} & (\tilde{H}_j + \tilde{\delta}_j^{n+1}) - (H_j + \delta_j^n) + \\ & \frac{3}{2}\xi \left(\bar{v}_j(\tilde{H} + \tilde{\delta}^n)(H_j + \delta_j^n) - \bar{v}_{j-1}(\tilde{H} + \tilde{\delta}^n)(H_{j-1} + \delta_{j-1}^n) \right) - \\ & \frac{1}{2}\xi \left(\bar{v}_j(\tilde{H} + \tilde{\delta}^{n-1})(H_j + \delta_j^{n-1}) - \bar{v}_{j-1}(\tilde{H} + \tilde{\delta}^{n-1})(H_{j-1} + \delta_{j-1}^{n-1}) \right) = a_s. \end{aligned} \quad (54)$$

After linearization around the steady state, insertion of Fourier modes, and simplification we arrive at

$$\tilde{\delta}_\omega^{n+1} = \delta_\omega^n - \xi \left(\frac{3}{2}(\nu \delta_\omega^n + \mu \tilde{\delta}_\omega^n) - \frac{1}{2}(\nu \delta_\omega^{n-1} + \mu \tilde{\delta}_\omega^{n-1}) \right). \quad (55)$$

Stability is investigated by writing the combined scheme AB-FAM with a companion matrix \mathbf{A}

$$\boldsymbol{\delta}^{n+1} = \mathbf{A} \boldsymbol{\delta}^n. \quad (56)$$

For stability, the eigenvalues λ_k of $\mathbf{A}(\mu, \nu, \xi)$ should satisfy $|\lambda_k(\mathbf{A})| \leq 1$ for all k and for all $\omega \Delta x \in [0, \pi]$. The companion matrix $\mathbf{A}^{2F}(\mu, \nu, \xi)$ and $\boldsymbol{\delta}^n$ for AB-FAM are

$$\mathbf{A}^{2F} = \begin{pmatrix} A_{11} & -\frac{1}{2}\xi\gamma\mu(1 - \frac{3}{2}\xi\mu) & -\frac{1}{4}\xi^2\gamma\mu\nu & -\frac{1}{4}\xi^2\gamma\mu^2 \\ 1 - \frac{3}{2}\xi\nu & -\frac{3}{2}\xi\mu & \frac{1}{2}\xi\nu & \frac{1}{2}\xi\mu \\ 1 & 0 & 0 & 0 \\ 0 & 1 & 0 & 0 \end{pmatrix}, \quad (57)$$

$$A_{11} = \gamma(1 - \frac{1}{2}\xi\nu - \frac{1}{2}\xi\mu(1 - \frac{3}{2}\xi\nu)), \quad (\boldsymbol{\delta}^n)^T = (\delta_\omega^n, \tilde{\delta}_\omega^n, \delta_\omega^{n-1}, \tilde{\delta}_\omega^{n-1}).$$

Here the superscript $2F$ denotes a second order fully implicit scheme.

If we instead consider SAM for $\bar{H}_j + \delta_j^{n+1}$, (49) is replaced by

$$\begin{aligned} & (\bar{H}_j + \delta_j^{n+1}) - (\bar{H}_j + \delta_j^n) + \\ & \frac{1}{2}\xi \left(\bar{v}_j(\bar{H} + \tilde{\delta}^{n+1})(\bar{H}_j + \tilde{\delta}_j^{n+1}) - \bar{v}_{j-1}(\bar{H} + \tilde{\delta}^{n+1})(\bar{H}_{j-1} + \tilde{\delta}_{j-1}^{n+1}) \right) + \\ & \frac{1}{2}\xi \left(\bar{v}_j(\bar{H} + \tilde{\delta}^n)(\bar{H}_j + \delta_j^n) - \bar{v}_{j-1}(\bar{H} + \tilde{\delta}^n)(\bar{H}_{j-1} + \delta_{j-1}^n) \right) = a_s. \end{aligned} \quad (58)$$

Proceeding as we did for AB-FAM we obtain the following companion matrix \mathbf{A}^{2S} for AB-SAM

$$\mathbf{A}^{2S} = \begin{pmatrix} A_{11} & -\frac{1}{2}\xi\mu(1 - \frac{3}{2}\xi(\mu + \nu)) & -\frac{1}{4}\xi^2\nu(\mu + \nu) & -\frac{1}{4}\xi^2\mu(\mu + \nu) \\ 1 - \frac{3}{2}\xi\nu & -\frac{3}{2}\xi\mu & \frac{1}{2}\xi\nu & \frac{1}{2}\xi\mu \\ 1 & 0 & 0 & 0 \\ 0 & 1 & 0 & 0 \end{pmatrix}, \quad (59)$$

with $A_{11} = 1 - \frac{1}{2}\xi\nu - \frac{1}{2}\xi(\mu + \nu)(1 - \frac{3}{2}\xi\nu)$.

The first order methods FE-FBE and FE-SBE have the following companion matrices, respectively,

$$\mathbf{A}^{1F} = \begin{pmatrix} A_{11} & \xi^2\mu^2\gamma \\ 1 - \xi\nu & -\xi\mu \end{pmatrix}, \quad A_{11} = \gamma(1 - \xi\mu(1 - \xi\nu)), \quad (60)$$

$$\mathbf{A}^{1S} = \begin{pmatrix} A_{11} & \xi^2\mu(\nu + \mu) \\ 1 - \xi\nu & -\xi\mu \end{pmatrix}, \quad A_{11} = 1 - \xi(\nu + \mu)(1 - \xi\nu), \quad (61)$$

with $(\delta^n)^T = (\delta_\omega^n, \delta_{*\omega}^n)$.

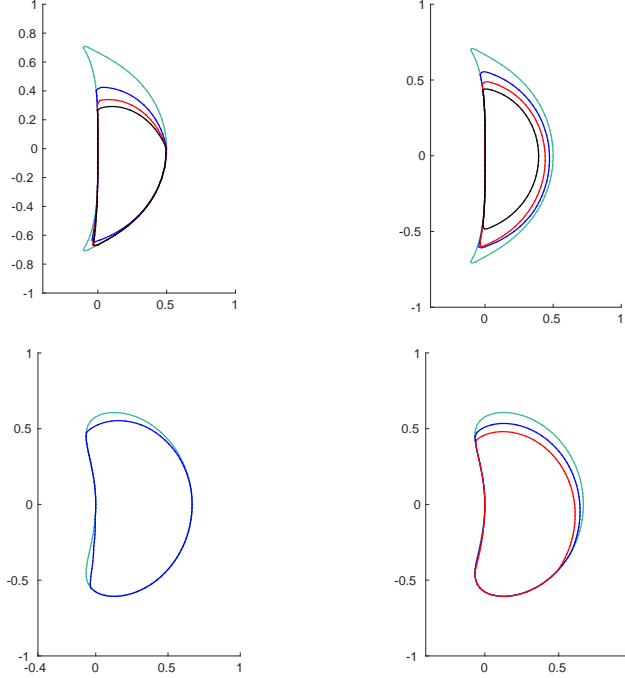


Figure 3: Stability regions for AB-FAM, AB-SAM, FE-FBE, and FE-SBE in the complex $\xi\mu$ -plane for different $\xi\bar{v}$. $\Re\xi\mu$ is on the x -axis and $\Im\xi\mu$ is on the y -axis. The values of $\xi\bar{v}$ increase in the order green, blue, red, black. Upper row: AB-FAM, $\xi\bar{v}$ is 0,1,2,3, (left), AB-SAM, $\xi\bar{v}$ is 0,0.2,0.4,0.6, (right). Lower row: FE-FBE, $\xi\bar{v} = 0, 5$, (left), FE-SBE, $\xi\bar{v} = 0, 0.2, 0.4$, (right).

The stability regions of AB-FAM, AB-SAM, FE-FBE, and FE-SBE where $\max_{k,\omega,\Delta x} |\lambda_k(\mathbf{A}(\mu, \nu, \xi))| \leq 1$ are found in Figure 3. The time step Δt has to be chosen such that $\xi\mu$ is inside the region for $\xi\bar{v}$.

The stability regions for fully implicit AB-FAM and FE-FBE converge when $\xi\bar{v}$ increases but AB-SAM is unstable for all μ when $\xi\bar{v} > 0.854$ and FE-SBE is unstable for all μ when $\xi\bar{v} > 0.5$. Since $\mu \propto 1/\Delta x$ and $\xi\mu \propto 1$ for stability, there is a time step constraint $\Delta t/\Delta x^2 \propto 1$ in all methods.

The predictor-corrector method for time integration is designed such that only one solution of the velocity field is necessary in every time step of length Δt_{pc} . A genuinely implicit method would be stable for a longer Δt_{impl} but a velocity solution then has to be computed in each iteration to solve a system of non-linear equations involving both H and \mathbf{v} . Suppose that n_{it} iterations are necessary in the non-linear solver of the thickness advection equation and that the work W_{vel} to compute the velocity completely dominates in the

algorithm for ice simulation. The total work in a time interval of length T is then $W_{\text{vel}}T/\Delta t_{\text{pc}}$ with the predictor-corrector scheme and $n_{\text{it}}W_{\text{vel}}T/\Delta t_{\text{impl}}$ with the genuinely implicit scheme.

Consider the first order methods FBE in (18) and SBE in (19) with time steps Δt_{impl} and Δt_{pc} , respectively. They have the same absolute value of the leading term in the local error $c_{\text{BE}}\Delta t^2$ for some $c_{\text{BE}} > 0$ in (23). The error tolerance ϵ is satisfied if $\Delta t_{\text{pc}} = \Delta t_{\text{impl}} = \sqrt{\epsilon}/c_{\text{BE}}$. The implicit FBE has no bound on Δt_{impl} for stability. The stability bound for SBE is $\Delta t_{\text{pc}} = c_{\text{stab}}\Delta x^2$ for some problem dependent $c_{\text{stab}} > 0$. Thus, stable and accurate time steps satisfy

$$\frac{\Delta t_{\text{pc}}}{\Delta t_{\text{impl}}} = \min\left(\frac{c_{\text{stab}}\Delta x^2\sqrt{c_{\text{BE}}}}{\sqrt{\epsilon}}, 1\right). \quad (62)$$

If Δx is large and ϵ is small, then $\Delta t_{\text{pc}} = \Delta t_{\text{impl}}$ and the time steps of both methods are restricted by the accuracy. On the other hand, when $\Delta t_{\text{pc}}/\Delta t_{\text{impl}} < 1$ then stability bounds Δt_{pc} . By (62) the computational work W for the two methods fulfills

$$\frac{W_{\text{impl}}}{W_{\text{pc}}} = n_{\text{it}} \min\left(\frac{c_{\text{stab}}\Delta x^2\sqrt{c_{\text{BE}}}}{\sqrt{\epsilon}}, 1\right). \quad (63)$$

If Δx is small and ϵ large, then the quotient in (63) may be less than 1 and the fully implicit FBE is the best choice depending on n_{it} and the problem specific parameters c_{BE} and c_{stab} .

7 Numerical results

Three numerical experiments are carried out here with the step size control in Section 4. The ice is assumed to be a homogeneous isotropic, isothermal material with a constant \mathcal{A} in (3). The top surface is stress free (10) and the bottom of the ice is frozen on the bedrock with (9) as the boundary condition. The physical parameters of the ice are given in Table 2.

Parameter	Quantity
$\rho = 910 \text{ kg m}^{-3}$	Ice density
$g = 9.81 \text{ m s}^{-2}$	Acceleration of gravity
$\mathcal{A} = 100 \text{ MPa}^{-3}\text{a}^{-1}$	Rate factor in flow law

Table 2: The physical parameters of ice.

In Experiment 1, the ice flow is solved by SIA. We compare the four schemes in Table 1 and relate the results to the analysis in Section 5. In Experiment

2, a 2D flow-line model of an ice sheet is solved by both SIA and FS. The efficiency of the adaptive time stepping method is evaluated in the transient simulation. Finally in Experiment 3, the adaptive time stepping method is tested on a 3D ice sheet model with FS and ISCAL running for more than 25,000 years.

7.1 Experiment 1 - 2D slab-on-slope experiment

7.1.1 Setup

As in the analysis in Section 5, a 2D slab-on-slope case is considered. Periodical boundary conditions are imposed on the left and right boundaries to represent an infinitely long slab. The computational domain is $L = 1000$ km with a uniform mesh size $\Delta x = 10$ km. The slope angle is $\alpha = -0.05$ and the steady state thickness of the slab is $H = 1000$ m with an initial perturbation $\delta(x) = 10 \sin(20\pi x/L)$ m at $t = 0$. The accumulation rate on the top surface is a constant $a_s = 0.3$ m/year or m/a. There is no melting or sliding at the bottom of the slab.

The velocities are computed by using the analytical solutions of SIA in (11) and the surface evolution is governed by the thickness equation (13). We use a finite difference method with an upwind scheme for the spatial discretization since this scheme in this case is identical to the finite element method with the chosen stabilization.

The adaptive time stepping methods in Table 1 are implemented in MATLAB in this experiment. The maximal Δt is estimated in every time step during the whole simulation according to the analysis in Section 5.2. The maximal Δt for the first order methods are estimated numerically by the Fourier analysis of the θ -method in (45) with $\theta = \frac{1}{5}$, i.e. implicit solution of the thickness equation. The estimated step sizes for the second order methods are computed from a similar analysis with $\theta = \frac{1}{10}$ in (45) giving equal weights to the explicit and implicit first derivatives in the thickness equation.

7.1.2 Results

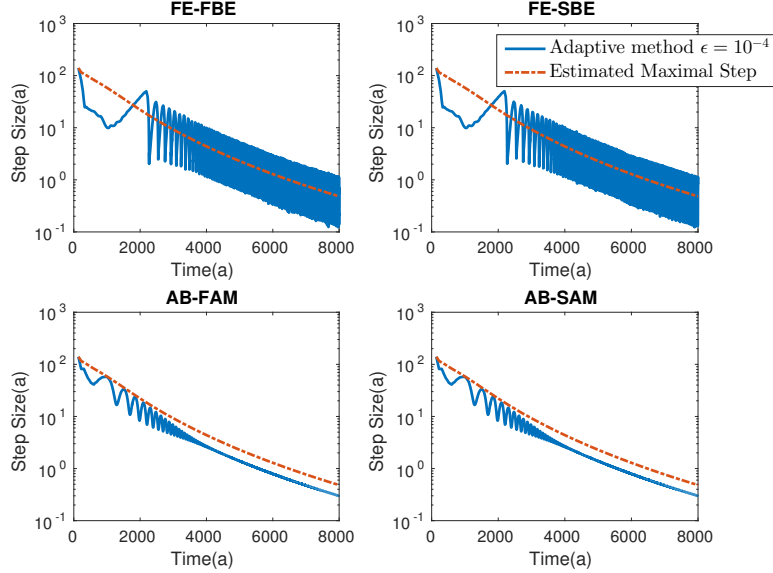


Figure 4: The time steps of the first and second order methods in the 2D slab-on-slope experiment with a tolerance $\epsilon = 10^{-4}$. The actual step sizes taken in the experiments are in solid blue. The estimated maximal step sizes of the corresponding θ -methods are in dashed red with $\theta = 1/5$ for FE-FBE and FE-SBE, and $\theta = 1/10$ for AB-FAM and AB-SAM. Upper row: FE-FBE (left) and FE-SBE (right). Lower row: AB-FAM (left) and AB-SAM (right).

The semi-implicit schemes FE-FBE and AB-FAM are compared with the fully implicit schemes FE-SBE and AB-SAM in Figure 4. All four experiments have the same error tolerance $\epsilon = 10^{-4}$ and are terminated at $T = 8000$ years. The controlled steps follow the estimated maximal steps of the corresponding θ -method. The coupled equation (32) always contains a diffusion term which is discretized explicitly in time restricting the time step, even for a fully implicit method with $\theta = \frac{1}{5}$ in (44).

In this experiment $\xi\bar{v} \approx 10^{-3}$ and $\Re\xi\mu$ oscillates between 10^{-3} to 10^1 . The time steps decrease with increasing time in all cases as the thickness of the ice grows from 1000 m to about 3400 m after 8000 years. Since $\xi\bar{v}$ is small, the stability bound on Δt is such that $\xi\mu \propto 1$ for all methods in Section 6. In (51) and B, $\mu \propto \bar{H}^4$ and consequently $\Delta t \propto \bar{H}^{-4}$ reducing Δt from about 130 at $t = 0$ to $130/3.4^4 \approx 1$ at $t = 8000$. All the four methods in Figure 3 are in this case almost at their maximum stability region (shown in green when $\xi\bar{v}$ is small) and Δt is restricted by $\xi\mu$ in the control method.

There are no significant differences in the stable step sizes between the semi-implicit and fully implicit methods for schemes of the same order. However, the semi-implicit methods are computationally cheaper than the fully implicit methods. Therefore, the semi-implicit FE-SBE and AB-SAM methods are used in the following experiments for efficiency reasons.

The time step in the first order methods (FE-SBE and FE-FBE) starts oscillating in magnitude after it reaches the estimated maximal steps. The oscillation is centered around the estimated maximal Δt . Figure 5 illustrates the estimated errors and step sizes for the FE-SBE method with an error tolerance from $\epsilon = 10^{-3}$ to $\epsilon = 10^{-6}$. The reference step sizes are computed by the same analysis as in Figure 4.

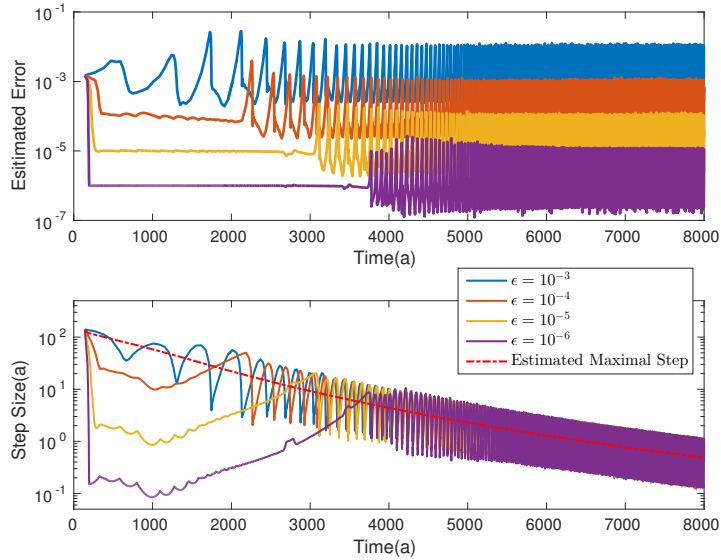


Figure 5: The 2D slab-on-slope experiment using the first order adaptive time stepping method (FE-SBE). The velocity field is computed by SIA. The maximal step sizes (red dashed) are estimated by using the analysis for θ -method with $\theta = 1/5$. The estimated errors (top) are computed by (24). The step sizes (bottom) are the steps taken in the simulations.

For the cases $\epsilon < 10^{-3}$, the estimated errors converge to their controlled tolerances immediately by reducing the time step. The estimated error stays constant at ϵ until Δt becomes constrained by the stability condition. The red dashed line indicates the maximal time step for stability by using the θ -method in solving the thickness equation (33). During the period where the error stays constant, the stability criterion is always satisfied, and Δt is bounded by the accuracy requirement. On the other hand, the time step

starts to oscillate when the value of $\xi\mu$ moves out from the stability region of Figure 3. In the case $\epsilon = 10^{-3}$, the oscillation starts immediately at the beginning of the simulation since the stability condition is the strongest in the whole interval under this ϵ .

The reason for the oscillation in the size of the time step is that the adaptive method will try to use longer time steps as long as the estimated accuracy requirements are fulfilled. The PI controller increases Δt a few times even if it violates the local stability criterion. The instability will not appear immediately in the controlled error but after a short time the instability is detected in the error estimate and the time step is reduced. When the size of the time step starts to oscillate, it is controlled by stability. When Δt is bounded by stability it is the same for all values of ϵ and it follows the shape of the theoretical stability bound. Note that the size of Δt is plotted in a logarithmic scale which means that the absolute amplitude of the oscillation decreases with time.

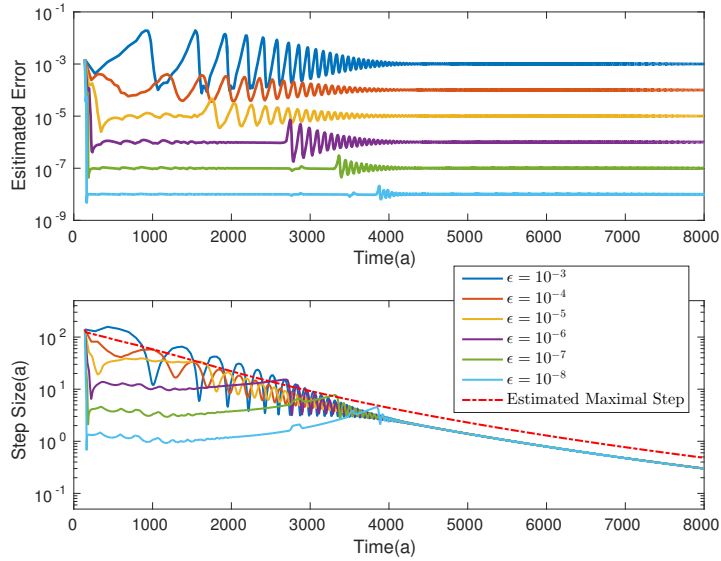


Figure 6: The 2D slab-on-slope experiment using second order adaptive time stepping method (AB-SAM). The velocity field is computed by SIA. The maximal step sizes (red dashed) are estimated by using the analysis for θ -method. The estimated errors (top) are computed by (28). The step sizes (bottom) are the steps taken in the simulations.

The behavior of the second order method AB-SAM before the oscillations in Δt in Figure 6 is similar to the first order method FE-FBE. The time step is first bounded by the accuracy criterion and then by the stability criterion

when the thickness of the ice grows. When the stability bound is reached we see oscillations also here, but the amplitudes are smaller than in the first order case and the oscillations are damped.

7.2 Experiment 2 - two dimensional moving margin experiment

One advantage of using an adaptive time stepping method is the efficiency in transient simulations compared to using a constant minimal Δt in the whole interval. Since the time step is automatically adjusted with respect to accuracy and stability, we are able to use as large time steps as possible with respect to both accuracy and stability everywhere in the interval.

7.2.1 Setup

In this experiment, a 2D moving margin experiment is performed to test the adaptive time stepping method with FS and SIA in Elmer/Ice. The length of the ice sheet is $L = 1000$ km. The accumulation rate is defined by

$$a_s = \max(0, \min(0.5, s(R - |x - 0.5L|))),$$

where $s = 10^{-5} \text{ a}^{-1}$ and $R = 2 \times 10^5$ m. The initial thickness of the ice is $H(x, 0) = 100$ m in the whole domain. The mesh size is $\Delta x = 1.25$ km in the horizontal direction with 5 vertical extruded layers which appears to be sufficient in our experiments. FS is solved by the Stokes solver in Elmer/Ice [19] with a convergence tolerance 10^{-6} for the nonlinear system and a direct solver for the linear system. Also, the SIA solver is the one implemented by Ahlkrona in Elmer/Ice [14].

7.2.2 Results

The second order AB-SAM adaptive time stepping method is run for both SIA and FS system for about 2000 years in Figure 7. The three SIA cases behave similarly as in Experiment 1 (Figure 6). The size of the time step starts to oscillate as the ice grows thicker, after a while the amplitude of the oscillations decreases, and finally Δt converges to the same size for all values of the control ϵ when the time step is restricted by stability only. The bound on Δt in (43) decreases when H of the ice cap grows and the slope α of the ice margin increases. In the FS cases, the size of the step is controlled by accuracy in the whole period, while the stability is automatically maintained by the adaptive method.

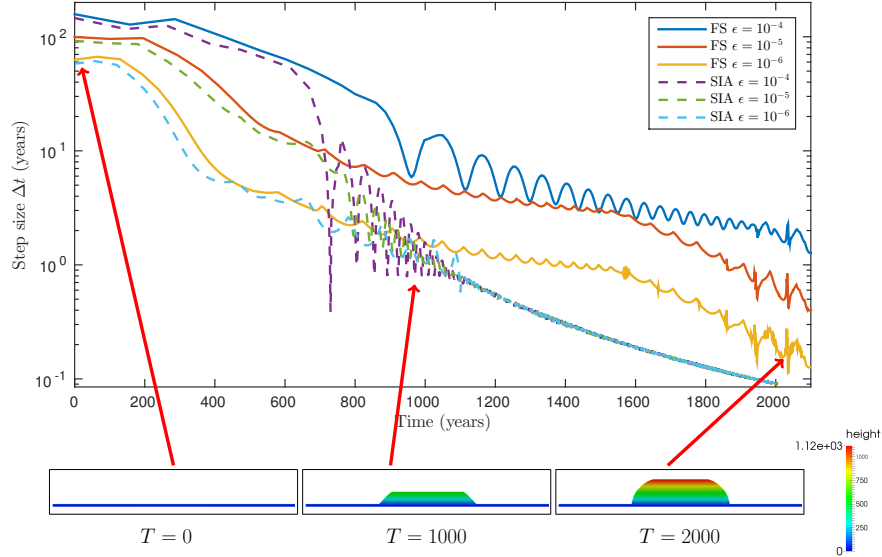


Figure 7: The 2D moving margin experiment with the AB-SAM method for different tolerances with $\Delta x = 1.25$ km solved by Elmer/Ice using SIA or FS. The error tolerance ϵ used in the time adaptive method is 10^{-4} , 10^{-5} , and 10^{-6} . The three figures at the bottom show the height of the ice cap at three time points. The y -axis in these figures is scaled by a factor of 100 compared to the x -axis.

The average step sizes of the FS cases are 6.55, 3.48 and 1.08 years for $\epsilon = 10^{-4}$, 10^{-5} , and 10^{-6} . With a constant time step, Δt would have been the smallest one in the interval, i.e. 1.72, 0.51 and 0.14 years, respectively. The initial time step is reduced by more than two orders of magnitude. Also, we would have had to guess the size of a constant time step to achieve a certain accuracy which is virtually impossible. The efficiency using FS is improved by at least a factor of 4 (which is the ratio between average step sizes of constant time stepping method and the adaptive method) without losing stability and in control of the accuracy.

7.3 Experiment 3 - EISMINT 3D with ISCAL

7.3.1 Setup

The capability of handling a 3D ice sheet model is tested in Elmer/Ice in this experiment. The computational domain is 1500×1500 km² with a Cartesian grid ($\Delta x = 60$ km) on the horizontal plane and extruded into 5 layers in the

vertical direction. The initial thickness of the ice is $H(x, 0) = 10$ m in the whole domain. The minimal ice thickness is also limited to 10 m to avoid negative thickness or hanging nodes by melting. The accumulation/ablation rate is

$$a_s = \min(0.5, s(R - d)),$$

where

$$d = \sqrt{(x - x_{\text{center}})^2 + (y - y_{\text{center}})^2},$$

$s = 10^{-5}$ a $^{-1}$ and $R = 2 \times 10^5$ m. This is the same configuration as the moving margin experiment in EISMINT 3D benchmark test [32, 38].

The problem is first solved by FS with constant time steps ($\Delta t = 5$ a) for 12 initial steps and then by the second order AB-SAM adaptive time stepping method to the steady state. The tolerance is set to $\epsilon = 10^{-3}$. Finally, the combination of ISCAL and AB-SAM is tested with the steady state solution of the FS simulation as the spin-up solution. The linear system is solved by the Generalized Conjugate Residual method in Elmer/Ice with a tolerance 10^{-12} and the convergence tolerance for non-linear solver is set to 10^{-6} . The tolerance on the relative error in ISCAL is 5% and the tolerance on the absolute error is 10 m/a. These tolerances control the switch between the FS and SIA equations in [17].

7.3.2 Results

The result from the transient simulation is shown in Figure 8. At $T = 60$ a, the ice is thin and flat. Therefore, the step size taken by the adaptive method grows quickly and reaches about 1000 a. At $T \approx 3900$ a when the ice cap is formed, the local truncation error exceeds the tolerance. Then, the step size decreases to satisfy stability and accuracy requirements at the steep margin slope (where $\partial h / \partial x$ is large) and the thick ice dome in the ice cap (where H is large) as shown in (43). The estimated local truncation error returns to the tolerance level and oscillates around it until the steady state is reached at $T \approx 10000$ a.

The solution from the transient simulation is used as input to a steady-state simulation using ISCAL. The estimated local truncation errors and the time steps are shown in Figure 9 for the error tolerances $\epsilon = 10^{-2}$, 10^{-3} , and 10^{-4} . The average step size for $\epsilon = 10^{-2}$ is 12.41 years whereas it is 8.10 years in the case $\epsilon = 10^{-3}$ and 7.99 years for $\epsilon = 10^{-4}$. Although the step size oscillates in the whole simulation, the solution is in all cases stable and accurate. Combining ISCAL [17] and our proposed adaptive time stepping method provides a stable, efficient and accurate solution for the steady-state EISMINT 3D experiment over 25,000 years.

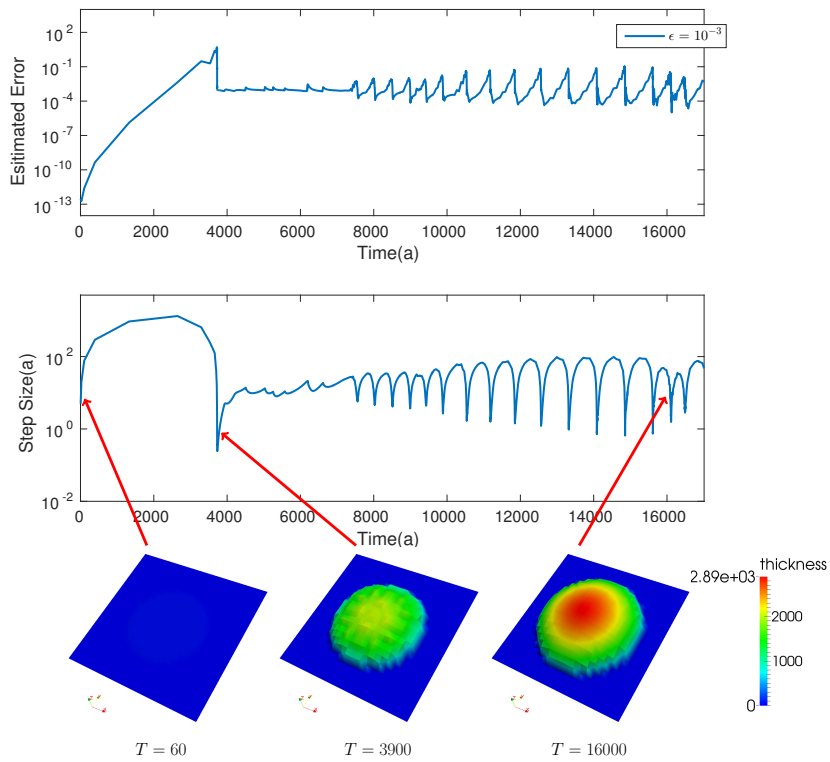


Figure 8: The EISMINT 3D experiment ($\Delta x = 60$ km) solved by FS and the second order AB-SAM adaptive time stepping method for the transient simulation. The three figures at the bottom display the thickness of the ice at $T = 60$, 3900 and 16000 years.

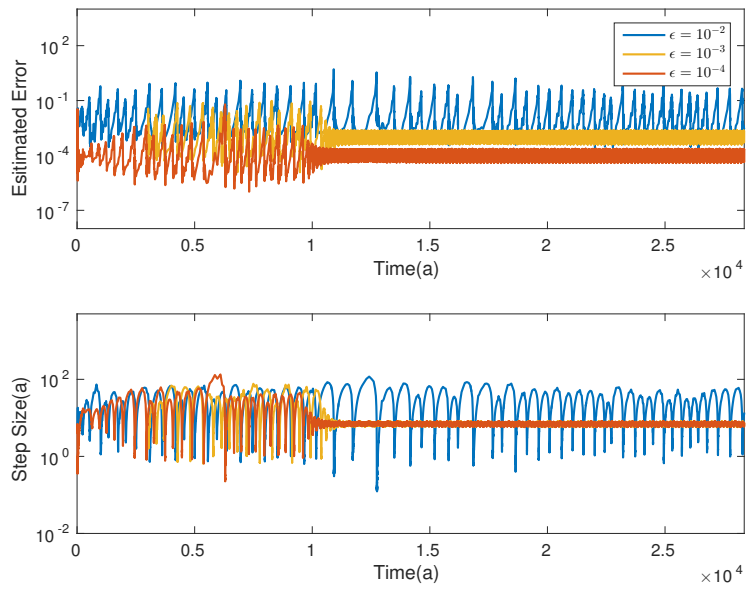


Figure 9: The EISMINT 3D experiment ($\Delta x = 60$ km) with second order AB-SAM adaptive time stepping method for steady states. The problem is simulated by Elmer/Ice using the ISCAL method. The initial condition is the ice cap at $T = 16000$ in Figure 8.

8 Conclusions and discussion

With a constant time step Δt in the whole time interval of interest, we have to take the minimal one in the interval for stability. The accuracy of the approximation of the time derivative is difficult to assess *a priori* with a fixed time step. Instead, a time step control is proposed and tested here for the shallow ice approximation (SIA), the full Stokes (FS) equation, the combination of them in ISCAL, and the thickness advection equation. The stability of the numerical solution is maintained and the accuracy is controlled by keeping the local error below a given threshold. Depending on the threshold, Δt is bound by stability requirements or accuracy requirements.

The most expensive part of the simulations is to determine the velocity field in the ice in each time step. To solve the FS equations is very costly, ISCAL is less expensive, and SIA is fairly cheap but still much more computationally expensive than solving the thickness advection equation in one dimension lower. We have developed a method advancing the solution in time and estimating the time discretization error requiring only one solution of the velocity field per time step. The method takes a shorter Δt than an implicit method but with less work in each time step and the solver is simpler. Our method is applied to the simulation of a 2D ice slab and a 3D circular ice sheet. The stability bounds in the experiments are explained by and agree well with the theoretical results.

Acknowledgment

This work has been supported by FORMAS grant 2013-1600 to Nina Kirchner. The computations were performed on resources provided by SNIC through Uppsala Multidisciplinary Center for Advanced Computational Science (UPPMAX) and PDC Center for High Performance Computing at KTH. Thanks to Josefin Ahlkrona for careful reading of a draft of the paper.

References

- [1] R. B. Alley, P. U. Clark, P. Huybrechts, I. Joughin, Ice-sheet and sea-level change, *Science* 310 (2005) 456–460.
- [2] R. M. DeConto, D. Pollard, Contribution of Antarctica to past and future sea-level rise, *Nature* 531 (2016) 591–597.

- [3] E. Hanna, F. J. Navarro, F. Pattyn, C. M. Domingues, X. Fettweis, E. R. Ivins, R. J. Nicholls, C. Ritz, B. Smith, S. Tulaczyk, P. L. Whitehouse, H. J. Zwally, Ice-sheet mass balance and climate change, *Nature* 498 (2013) 51–59.
- [4] D. G. Vaughan, R. Arthern, Why is it hard to predict the future of ice sheets?, *Science* 315 (2007) 1503–1504.
- [5] D. Pollard, R. M. DeConto, Modelling West Antarctic ice sheet growth and collapse through the past five million years, *Nature* 458 (2009) 329–332.
- [6] H. Seddik, R. Greve, T. Zwinger, F. Gillet-Chaulet, O. Gagliardini, Simulations of the Greenland ice sheet 100 years into the future with the full Stokes model Elmer/Ice, *J. Glaciol.* 58 (2012) 427–440.
- [7] C. R. Stokes, L. Tarasov, R. Blomdin, T. M. Cronin, T. G. Fisher, R. Gyllencreutz, C. Hättstrand, J. Heyman, R. C. A. Hindmarsh, A. L. C. Hughes, M. Jakobsson, N. Kirchner, S. J. Livingstone, M. Margold, J. B. Murton, R. Noormets, W. R. Peltier, D. M. Peteet, D. J. W. Piper, F. Preusser, H. Renssen, D. H. Roberts, D. M. Roche, F. Saint-Ange, A. P. Stroeven, On the reconstruction of palaeo-ice sheets: Recent advances and future challenges, *Quat. Sci. Rev.* 125 (2015) 15–49.
- [8] D. R. Baral, K. Hutter, R. Greve, Asymptotic theories of large-scale motion, temperature and moisture distribution in land-based polythermal ice sheets: A critical review and new developments, *Appl. Mech. Rev.* 54 (2001) 215–256.
- [9] K. Hutter, *Theoretical Glaciology*, D. Reidel Publishing Company, Terra Scientific Publishing Company, Dordrecht, 1983.
- [10] M. Weis, R. Greve, K. Hutter, Theory of shallow ice shelves, *Continuum Mech. Thermodyn.* 11 (1999) 15–50.
- [11] D. R. MacAyeal, Large-scale ice flow over a viscous basal sediment: Theory and application to Ice Stream B, Antarctica., *J. Geophys. Res.* 94 (1989) 4071–4078.
- [12] H. Blatter, Velocity and stress fields in grounded glaciers: a simple algorithm for including deviatoric stress gradients, *J. Glaciol.* 41 (1995) 333–344.
- [13] F. Pattyn, A new three-dimensional higher-order thermomechanical ice sheet model: Basic sensitivity, ice stream development, and ice flow across subglacial lakes, *J. Geophys. Res.* 108 (2003) 2382.

- [14] J. Ahlkrona, N. Kirchner, P. Lötstedt, Accuracy of the zeroth and second order shallow ice approximation - Numerical and theoretical results, *Geosci. Model Dev.* 6 (2013) 2135–2152.
- [15] R. Hindmarsh, A numerical comparison of approximations to the Stokes equations used in ice sheet and glacier modeling, *J. Geophys. Res.* 109 (2004) F01012.
- [16] E. le Meur, O. Gagliardini, T. Zwinger, J. Ruokolainen, Glacier flow modelling: a comparison of the Shallow Ice Approximation and the full-Stokes solution, *C. R. Phys.* 5 (2004) 709–722.
- [17] J. Ahlkrona, P. Lötstedt, N. Kirchner, T. Zwinger, Dynamically coupling the non-linear Stokes equations with the shallow ice approximation in glaciology: Description and first applications of the ISCAL method, *J. Comput. Phys.* 308 (2016) 1–19.
- [18] N. Kirchner, J. Ahlkrona, E. Gowan, P. Lötstedt, J. Lea, R. Noormets, L. von Sydow, J. Dowdeswell, T. Benham, Shallow ice approximation, second order shallow ice approximation, and full stokes models: A discussion of their roles in palaeo-ice sheet modelling and development, *Quater. Sci. Rev.* 135 (2016) 103 – 114. doi:<http://dx.doi.org/10.1016/j.quascirev.2016.01.013>.
- [19] O. Gagliardini, T. Zwinger, F. Gillet-Chaulet, G. Durand, L. Favier, B. de Fleurian, R. Greve, M. Malinen, C. Martín, P. Råback, J. Ruokolainen, M. Sacchetti, M. Schäfer, H. Seddik, J. Thies, Capabilities and performance of Elmer/Ice, a new generation ice-sheet model, *Geosci. Model Dev.* 6 (2013) 1299–1318.
- [20] F. Gillet-Chaulet, O. Gagliardini, H. Seddik, M. Nodet, G. Durand, C. Ritz, T. Zwinger, R. Greve, D. G. Vaughan, Greenland ice sheet contribution to sea-level rise from a new-generation ice-sheet model, *The Cryosphere* 6 (2012) 1561–1576.
- [21] E. Larour, H. Seroussi, M. Morlighem, E. Rignot, Continental scale, high order, high spatial resolution, ice sheet modeling using the Ice Sheet System Model (ISSM), *J. Geophys. Res.* 117 (2012) F01022.
- [22] W. Leng, L. Ju, M. Gunzburger, S. Price, A parallel computational model for three-dimensional, thermo-mechanical Stokes flow simulations of glaciers and ice sheets, *Commun. Comput. Phys.* 4 (2014) 1056–1080.
- [23] I. K. Tezaur, M. Perego, A. G. Salinger, R. S. Tuminaro, S. F. Price, Albany/FELIX: a parallel, scalable and robust, finite element, first-order Stokes approximation ice sheet solver built for advanced analysis, *Geosci. Model Dev.* 8 (2015) 1197–1220.

- [24] S. L. Cornford, D. F. Martin, D. T. Graves, D. F. Ranken, A. M. L. Brocq, R. M. Gladstone, A. J. Payne, E. G. Ng, W. H. Lipscomb, Adaptive mesh, finite volume modeling of marine ice sheets, *J. Comput. Phys.* 232 (2013) 529–549.
- [25] R. C. A. Hindmarsh, Notes on basic glaciological computational methods and algorithms, in: B. Straughan, R. Greve, H. Ehrentraut, Y. Wang (Eds.), *Continuum Methods and Applications in Geophysics and the Environment*, Springer, Berlin, 2001, pp. 222–249.
- [26] R. Greve, R. Calov, Comparison of numerical schemes for the solution of the ice-thickness equation in a dynamic/thermodynamic ice-sheet model, *J. Comput. Phys.* 179 (2002) 649–664.
- [27] E. Hairer, S. P. Nørsett, G. Wanner, *Solving Ordinary Differential Equations I, Nonstiff Problems*, 2nd Edition, Springer, Berlin, 1995.
- [28] E. Hairer, G. Wanner, *Solving Ordinary Differential Equations II, Stiff and Differential-Algebraic Problems*, 2nd Edition, Springer, Berlin, 1996.
- [29] G. Söderlind, Time-step selection algorithms: Adaptivity, control, and signal processing, *Appl. Numer. Math.* 56 (2006) 488–502.
- [30] G. Söderlind, L. Wang, Adaptive time-stepping and computational stability, *J. Comput. Appl. Math.* 185 (2006) 225–243.
- [31] M. Fujii, An extension of Milne’s device for the Adams predictor-corrector methods, *Japan J. Indust. Appl. Math.* 8 (1991) 1–18.
- [32] P. Huybrechts, A. J. Payne, the EISMINT intercomparison group, The EISMINT benchmarks for testing ice sheet models, *Ann. Glaciol.* 23 (1996) 1–12.
- [33] F. Pattyn, L. Perichon, A. Aschwanden, B. Breuer, B. de Smedt, O. Gagliardini, G. H. Gudmundsson, R. Hindmarsh, A. Hubbard, J. V. Johnson, T. Kleiner, Y. Konovalov, C. Martin, A. J. Payne, D. Pollard, S. Price, M. Rückamp, F. Saito, O. Souček, S. Sugiyama, T. Zwinger, Benchmark experiments for higher-order and full-Stokes ice sheet models (ISMIP-HOM), *The Cryosphere* 2 (2008) 95–108.
- [34] C. Schoof, Coulomb friction and other sliding laws in a higher-order glacier flow model, *Math. Mod. Meth. Appl. Sci.* 20 (2010) 157–189.
- [35] R. Greve, H. Blatter, *Dynamics of Ice Sheets and Glaciers, Advances in Geophysical and Environmental Mechanics and Mathematics (AGEM²)*, Springer, Berlin, 2009.

- [36] J. Ahlkrona, N. Kirchner, P. Lötstedt, A numerical study of scaling relations for non-Newtonian thin film flows with applications in ice sheet modelling, *Quart. J. Mech. Appl. Math.* 66 (2013) 417–435.
- [37] E. DiBenedetto, *Degenerate Parabolic Equations*, Springer, New York, 1993.
- [38] A. J. Payne, P. Huybrechts, A. Abe-Ouchi, R. Calov, J. L. Fastook, R. Greve, S. J. Marshall, I. Marsiat, C. Ritz, L. Tarasov, M. P. A. Thomassen, Results from the EISMINT model intercomparison: the effects of thermomechanical coupling, *J. Glaciol.* 46 (2000) 227–238.

A Stability criterion for simplified 2D-problem

Let $\kappa = \omega \Delta x$ and a replace $|a|$ in (41) and compute $|\lambda|^2$ for λ

$$\begin{aligned}
|\lambda|^2 &= (a - 2c)^2 + (1 - a - 2c)^2 + 8c^2 \cos^3 \kappa + 4c(1 - 2c) \cos^2 \kappa + \\
&\quad + (2a - 2a^2 - 8c^2) \cos \kappa \\
&= 8c^2 \cos^3 \kappa + (4c - 8c^2) \cos^2 \kappa + (2a - 2a^2 - 8c^2) \cos \kappa + \\
&\quad + 2a^2 + 8c^2 - 2a - 4c + 1.
\end{aligned} \tag{64}$$

To obtain $|\lambda|^2 \leq 1$ we need

$$(\cos \kappa - 1)(8c^2 \cos^2 \kappa + 4c \cos \kappa + 2a - 2a^2 - 8c^2 + 4c) \leq 0, \tag{65}$$

i.e. either $\cos \kappa = 1$ or

$$8c^2 \cos^2 \kappa + 4c \cos \kappa + 2a - 2a^2 - 8c^2 + 4c \geq 0. \tag{66}$$

By denoting

$$g(\kappa) = 8c^2 \cos^2 \kappa + 4c \cos \kappa + 2a - 2a^2 - 8c^2 + 4c, \tag{67}$$

the problem becomes to find κ^* that minimizes $g(\kappa)$ and then solve $|\lambda|^2 \leq 1$. Since $a > 0$, $c > 0$, the minimizing problem has the solution

$$\cos \kappa^* = -\frac{1}{4c},$$

and the inequality to solve for Δt becomes

$$8c^2 - 4c + 2a^2 - 2a + \frac{1}{2} \leq 0. \tag{68}$$

We only need to consider the case where $c \geq \frac{1}{4}$, since for $c < \frac{1}{4}$ the inequality holds for all Δt . Let $a = kc$ for $k > 0$ which in (68) gives

$$(8 + 2k^2)c^2 - (4 + 2k)c + \frac{1}{2} \leq 0, \tag{69}$$

i.e.

$$\frac{k+2-2\sqrt{k}}{2k^2+8} \leq c \leq \frac{k+2+2\sqrt{k}}{2k^2+8}. \quad (70)$$

Since $c \geq \frac{1}{4}$ and $k > 0$ only the right inequality becomes a restriction and we get

$$c \leq \frac{k+2+2\sqrt{k}}{2k^2+8}, \quad (71)$$

which gives

$$\Delta t \leq \frac{k+2+2\sqrt{k}}{2k^2+8} \frac{2\Delta x^2}{3C\alpha^2 H^5}. \quad (72)$$

B Dependence of \bar{v} on H in the discretization

The formula for \bar{v} at x_j for SIA in (30) with a discretized first derivative can be written

$$\bar{v} = -CH^4(\mathcal{D}h)_j^3 = (\mathcal{D}h)_j^3 G(H), \quad (73)$$

where $(\mathcal{D}h)_j$ is the discrete approximation of $\partial h/\partial x$ at x_j . Then the sensitivity $\partial\bar{v}/\partial H_j$ in Section 6 is

$$\frac{\partial\bar{v}}{\partial H_j} = (\mathcal{D}h)_j^3 \frac{G(H_j)}{\partial H_j} + \left(3(\mathcal{D}h)_j^2 \frac{\partial(\mathcal{D}h)_j}{\partial h_j} \frac{\partial h_j}{\partial H_j} \right) G(H_j). \quad (74)$$

All components on the right hand side of (74) are smooth and of $\mathcal{O}(1)$ except for $\partial(\mathcal{D}h)_j/\partial h_j$ which is of $\mathcal{O}(\Delta x^{-1})$. Therefore, $\partial\bar{v}/\partial H_j$ and μ in (51) are both of $\mathcal{O}(\Delta x^{-1})$ and potentially large for small Δx .